



Title	Complex Formation Behavior of Silica Nanoparticles and Xanthan
Author(s)	Tomofuji, Yu; Terao, Ken
Citation	Macromolecular Symposia. 2023, 408(1), p. 2200025
Version Type	AM
URL	https://hdl.handle.net/11094/91050
rights	© 2023 Wiley-VCH GmbH
Note	

The University of Osaka Institutional Knowledge Archive : OUKA

<https://ir.library.osaka-u.ac.jp/>

The University of Osaka

Complex Formation Behavior of Silica Nanoparticles and Xanthan*Yu Tomofuji and Ken Terao**

Y. Tomofuji, K. Terao

Department of Macromolecular Science, Graduate School of Science, Osaka University, 1-1 Machikaneyama-cho, Toyonaka, Osaka 560-0043, Japan

E-mail: terao.ken.sci@osaka-u.ac.jp

Keywords: nanoparticles; polysaccharides; electrostatic interactions; ζ potential; circular dichroism; light scattering**Abstract:**

Polyion complex formation between negatively charged polysaccharide, xanthan, and positively charged silica nanoparticles, Ludox CL, was investigated in an acetate buffer at pH 5.0. Appreciable precipitate was found in the composition range c_x/c_{SiNP} from 0.056 to 0.58, where c_x and c_{SiNP} are the mass concentrations of xanthan and silica nanoparticles, respectively. The sign change of the ζ potential for the mixed solutions was observed in the c_x/c_{SiNP} range. Significantly high scattering intensity was detected for the mixed solutions in a wider c_x/c_{SiNP} range, clearly showing the complex formation. The scattering profile measured by the small-angle X-ray scattering revealed that silica nanoparticles were packed loosely in the complex both when xanthan forms double helix and single chain conformations.

1. Introduction

Xanthan is an anionic polysaccharide which forms double helical structure in a dry sample,^[1-5] crystalline state,^[6] and aqueous solution^[7-9] at finite ionic strength. It thus behaves as a rigid rodlike chain with the Kuhn segment length L_K , a measure of the chain stiffness,^[10] of 240 nm in 100 mM aqueous NaCl.^[11] The double helical structure deforms to the single chain in low ionic strength aqueous solution with raising temperature^[12-15] with slow kinetics.^[16]

Xanthan can interact with positively charged silica nanoparticles (SiNPs) revealed by rheological properties.^[17] Some applications have been considered for the SiNP-xanthan

complex as an oil spill dispersant^[18] or a stabilizer of foam fluid^[19] whereas fundamental studies of the complex formation is still limited. We thus investigated intermolecular interactions of an alumina coated SiNP and xanthan in a buffer with low ionic strength to reveal the complex formation behavior of SiNP and xanthan.

2. Experimental Section

2.1. Sample and Solution Preparation

A xanthan sample purchased from TCI was sonicated to scission the main chain with keeping the double helical structure. It was further fractionated and purified in the manner reported previously.^[16] The resulting sodium salt xanthan sample designated as **X367k** was characterized by using a size-exclusion chromatography with light scattering and refractive index detectors as in the case of our recent study.^[16] The weight-average molar mass M_w and the dispersity index D ($\equiv M_w / M_n$, with M_n being the number average molar mass) were determined to be 367 kg mol^{-1} and 1.2, respectively. The acetate/pyruvate ratio was 1.5 determined from $^1\text{H NMR}$ in our previous study.^[16] SiNPs with alumina coating, Ludox CL, dispersed in water ($\sim 30 \text{ wt\%}$) at $\text{pH} = 4.5$, were purchased from Sigma Aldrich. This SiNP has mean radius of 8.6 nm ^[20] and positive ζ potential when pH is between 4 and 8,^[20, 21] but actual charge number is difficult to be determined. The actual concentration c_{SiNP} of the SiNP was estimated from the weight of the residue after lyophilization.

The **X367k** sample was dissolved in 10 mM acetate buffer at $\text{pH} 5.0$ including 10 mM NaCl to prepare the solution with the xanthan mass concentration $2c_x$, twice the concentration of the mixed solution. We chose the buffer instead of aqueous NaCl because the original Ludox CL has weak acidic pH of 4.5. The purchased aqueous SiNP solution ($\sim 30 \text{ wt\%}$) was diluted with the same buffer to obtain the solution with $2c_{\text{SiNP}}$. The two solutions were incubated at a certain temperature T_{mix} of room temperature ($\sim 25 \text{ }^\circ\text{C}$) or $80 \text{ }^\circ\text{C}$, at which xanthan conformation is double helix or mostly single chain, respectively. The solutions with the equivalent volume

were mixed at T_{mix} just before (~ 10 min) the following measurements to prepare mixed solution with c_x and c_{SiNP} since it is known that the complex formation for SiNP-collagen system takes around 10 min.^[22]

2.2. Electrophoretic Light Scattering (ELS)

ELS measurement was carried out for SiNP and mixed solutions by using an Otsuka zeta potential analyzer ELSZ-2 to determine the ζ potential assuming the equation for the spherical particle. Each measurement was examined at the temperature $T_{\text{meas}} = T_{\text{mix}}$ (20 °C or 80 °C) and changed to the other temperature (80 °C or 20 °C).

2.3. Circular Dichroism (CD)

CD measurement was examined by using a JASCO J-720WO spectropolarimeter. Rectangular quartz cells with the optical path length of 2 mm or 10 mm were set in a thermostated cell holder. Mixed and measurement temperatures are the same as the ELS measurement.

2.4. Static and Dynamic Light Scattering (SLS and DLS)

Both SLS and DLS measurements were made for the 4 times diluted solutions of that described in section 2.1 with an ALV/SLS/DLS-5000 light scattering photometer ranging in the scattering angle from 40° to 150° at 25 °C, corresponding to the magnitude q of the scattering vector from 0.01 to 0.03 nm⁻¹. Vertically polarized incident light was used from an Nd:YAG laser (250 mW) with the wavelength λ_0 in vacuum being 532 nm. It should be noted that the measurement at 80 °C was difficult with our equipment. The excess scattering intensity R_q at q was determined from SLS measurements. DLS measurements give the intensity autocorrelation function which was analyzed by the CONTIN method to evaluate the spectrum

$A(R_{H,app})$ at the apparent hydrodynamic radius $R_{H,app}$ calculated from the relaxation time at finite q and concentrations by means of the Stokes–Einstein equation with the solvent viscosity and temperature.

2.5. Small-angle X-ray Scattering (SAXS)

SAXS measurement was made for **X367k**, Ludox CL, and the mixed solution at the BL40B2 beamline in SPring-8. The wavelength λ_0 of the incident X-ray was set to be 0.1 nm. The scattered X-ray was detected by the PILATUS 3 2M. The sample-to-detector length (camera length) was about 4 m. Silver behenate was used to determine the beam center and the accurate camera length. The scattering intensity $I(q)$ of the scattered X-ray at q was calculated from the 2D image with the SAngler software.^[23] The $I(q)$ data were calibrated by the intensity of the direct beam measured between sample and the detector to compensate the fluctuation of the incident light and the transparency of the solution. Both the solutions and the buffer were measured with exactly the same quartz capillary cell (2 mm ϕ). The excess scattering intensity $\Delta I(q)$ was estimated as the difference in $I(q)$ between the solution and the solvent.

3. Results and Discussion

Figure 1 shows a photograph for the mixed solutions of Ludox CL and **X367k** in the buffer at room temperature in which c_{SiNP} was set to be 0.6 mg cm⁻³. Appreciable precipitant was found for the solutions ranging in the concentration ratio c_x/c_{SiNP} between 0.056 and 0.58. Precipitation is generally found for polyion complexes around the charge neutralization composition because excessive charge can stabilize the nano-sized complex. Indeed, the ζ potential for the mixed solutions plotted against the composition c_x/c_{SiNP} in Figure 2 has positive values for $c_x/c_{SiNP} < 0.03$ and negative values for $c_x/c_{SiNP} > 0.4$, independent of the mixed and measurement temperatures (T_{mix} and T_{meas}).

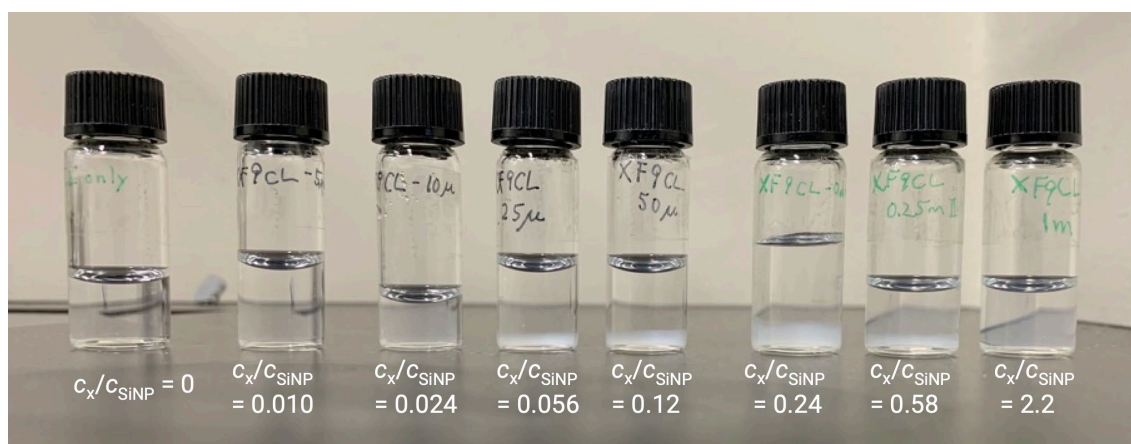


Figure 1. Photograph of mixed solutions of Ludox CL and xanthan in the pH 5.0 acetate buffer at indicated c_x/c_{SiNP} with $c_{\text{SiNP}} = 0.6 \text{ mg cm}^{-3}$.

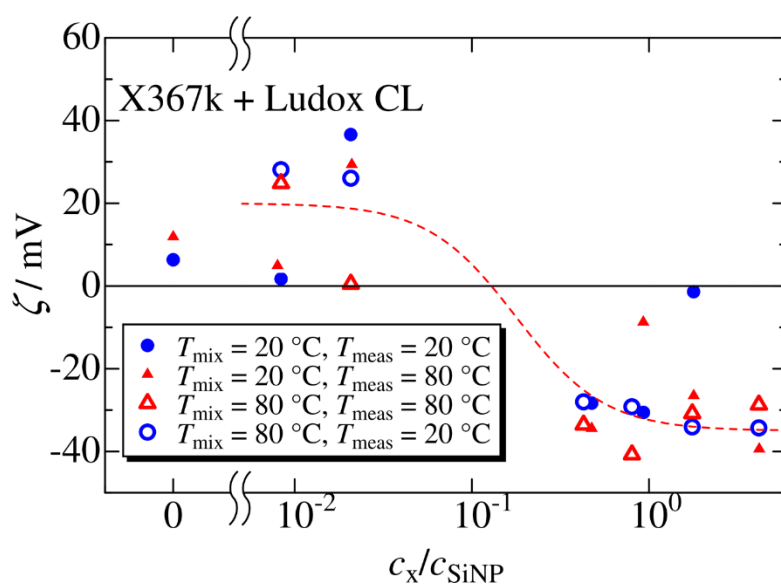


Figure 2. c_x/c_{SiNP} dependence of the ζ -potential for the mixed solutions of X367k and Ludox CL in the acetate buffer at indicated mixed temperature T_{mix} and the measurement temperature T_{meas} . A red dashed curve is eyeguides. $c_{\text{SiNP}} = 0.6 \text{ mg cm}^{-3}$.

To confirm the conformation of xanthan in the complex, CD spectra for xanthan with or without Ludox CL in the acetate buffer are compared in Figure 3. The ordinate specific ellipticity $[\theta]$, the ellipticity divided by the optical path length and c_x reflects the (side chain)

conformation of xanthan. Indeed, the $[\theta']$ data for $\lambda_0 < 225$ nm are appreciably different at the two measurement temperatures T_{meas} , at which xanthan forms double helical structure at 20 °C and most components become single chain at 80 °C.^[16] It can be seen from the figure that both the CD spectra are completely independent of c_{SiNP} , indicating that complex formation between xanthan and SiNP does not cause appreciable difference in the conformation of xanthan.

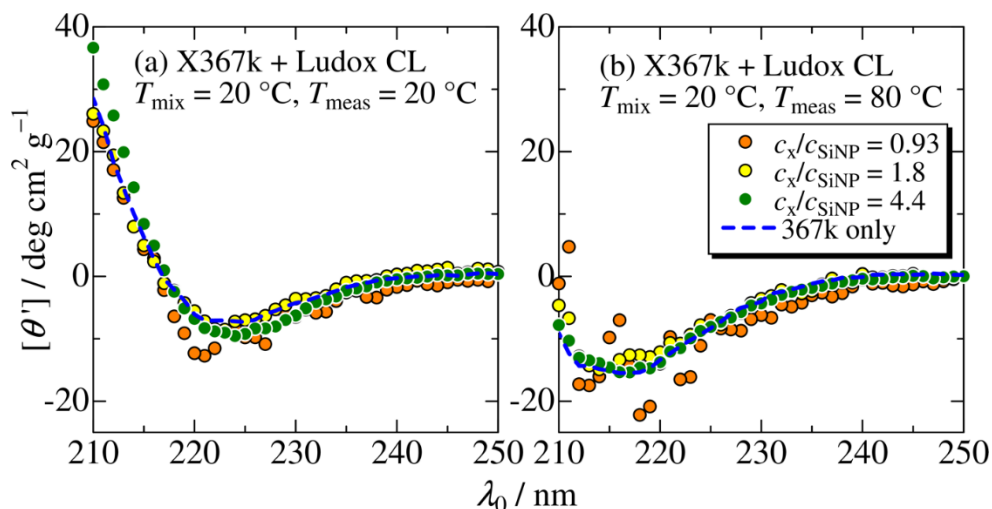


Figure 3. CD spectra for xanthan in the presence of SiNP with indicated c_x/c_{SiNP} . c_{SiNP} was set to be 0.6 mg cm^{-3} . (a) $T_{\text{mix}} = 20 \text{ °C}$, $T_{\text{meas}} = 20 \text{ °C}$. (b) $T_{\text{mix}} = 20 \text{ °C}$, $T_{\text{meas}} = 80 \text{ °C}$. Blue dashed curves denote the CD spectra for xanthan without SiNP.

As mentioned above, the mixed solution of SiNP and xanthan was turbid when $0.056 < c_x/c_{\text{SiNP}} < 0.58$. Considering that the electrostatic attraction is the dominant force to form the precipitation, complex formation can be still significant with excess amount of xanthan ($c_x/c_{\text{SiNP}} > 0.58$). Dynamic light scattering is one of the powerful methods to detect such small aggregates. Typical results for the DLS measurements are therefore displayed in Figure 4 in which the apparent spectrum $A(R_{\text{H,app}})$, which is proportional to the scattering intensity of each component, is plotted against the apparent hydrodynamic radius $R_{\text{H,app}}$. The bimodal peak for Ludox CL indicates slight number of huge aggregates of the SiNP in the buffer while the weight fraction of the aggregates is negligibly small. Furthermore, the averaged apparent

hydrodynamic radius $\overline{R_{H,app,s}}$ for the small component (54 nm) is much larger than the average radius of 8.6 nm,^[20] suggesting aggregates consisting in the order of 100 nanoparticles. Consequently, the reduced scattering intensity $R_{q,s}$ for the small component estimated from R_q and the area ratio of the spectrum in the manner reported previously^[24] are plotted in Figure 5. This Guinier plots has significantly large slope at low q region, showing that the radius of gyration R_g is larger than 100 nm, and hence, only few data points are evaluated in the Guinier region of $q R_g < 1.3$, indicating that accurate scattering intensity at $q = 0$ and R_g cannot be determined from the current light scattering data. On the other hand, the spectra for the mixed solutions have mostly monomodal peak for all investigated c_x/c_{SiNP} . Very small peak around 20 nm can be assigned to dispersed SiNPs. This is most likely because of the much higher scattering intensity of the mixed solutions as shown in Figure 5.

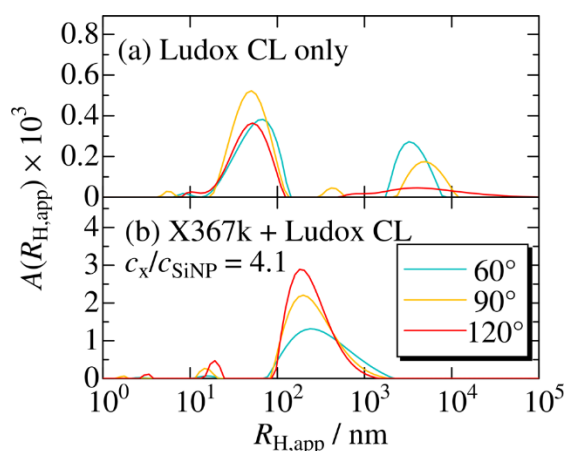


Figure 4. The distribution of the apparent hydrodynamic radius $A(R_{H,app})$ obtained by DLS for the mixed solutions of Ludox CL and X367k in the acetate buffer ($c_{SiNP} = 0.15 \text{ mg cm}^{-3}$) at 25 °C detected at the indicated scattering angle. (a) Ludox CL only, (b) $c_x/c_{SiNP} = 4.1$.

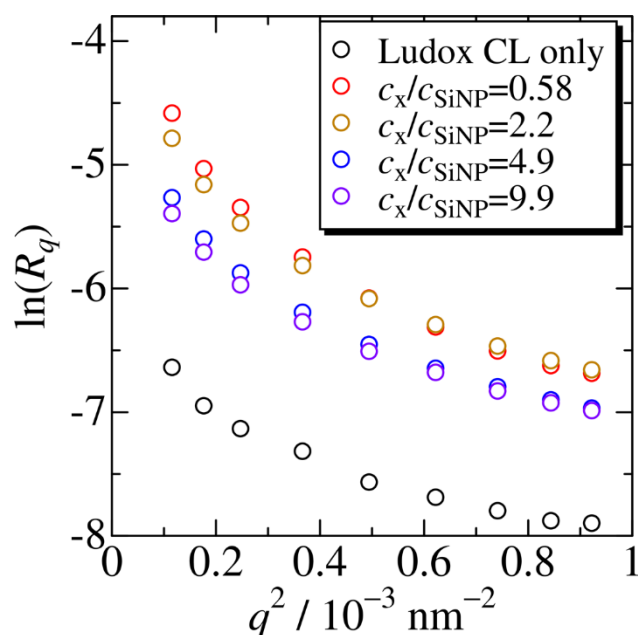


Figure 5. Guinier plots for the mixed solutions of Ludox CL and X367k at indicated in the acetate buffer ($c_{\text{SiNP}} = 0.15 \text{ mg cm}^{-3}$) at 25 °C.

Figure 6 illustrates the composition (c_x/c_{SiNP}) dependence of R_q at the lowest q of 0.0108 nm^{-1} and the averaged apparent hydrodynamic radius $\overline{R_{\text{H,app}}}$ (or $\overline{R_{\text{H,app,s}}}$ for the small component). The scattering intensity increases rapidly with lowering c_x/c_{SiNP} for all the mixed solutions. The R_q value at the lowest q in Figure 6(a) corresponds to the molar mass in the range of 10^5 kg mol^{-1} assuming that all components are included in the polyion complexes and the resulting complexes have the differential refractive index increment of $0.1 \text{ cm}^3 \text{ g}^{-1}$. The dashed red line in the panel corresponding to the molar mass of double helical xanthan is also much smaller than the data points. Taking into consideration that the lowest c_x/c_{SiNP} investigated is still higher than those for that observing the precipitation, the downward curvature is consistent with the light scattering results for the polyion complex composed of various kinds of polycations and polyanions.^[25, 26] Similar tendency was observed for the $\overline{R_{\text{H,app}}}$ (or $\overline{R_{\text{H,app,s}}}$) data while they are much larger than the double helical xanthan molecules; the dashed line in Figure 6(b) calculated from the cylinder model^[27] with the parameters by Sato et al.^[11]

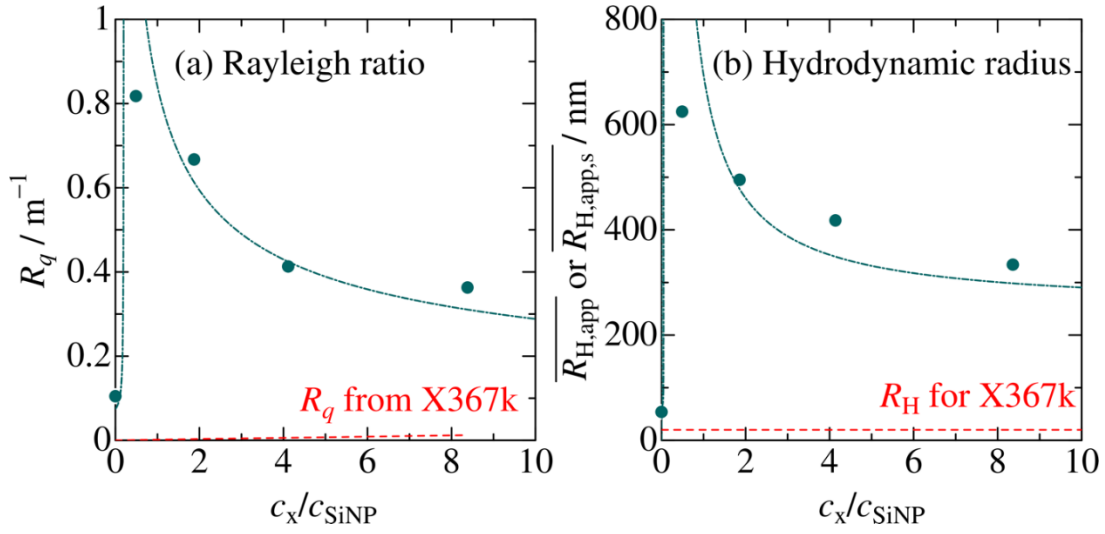


Figure 6. Analyzed light scattering data for (a) c_x/c_{SiNP} dependence of R_q (or $R_{q,s}$) at $q = 0.0108 \text{ nm}^{-1}$ with $c_{\text{SiNP}} = 0.15 \text{ mg cm}^{-3}$. Dashed line, calculated scattering intensity from xanthan molecularly dispersed in the buffer. (b) c_x/c_{SiNP} dependence of $\overline{R_{H,\text{app}}}$ (or $\overline{R_{H,\text{app},s}}$). Dashed line is the calculated values for double helical xanthan (see text).

Aggregation structure of nanoparticles can be more affectable to the scattering profiles in the higher q range. The excess scattering intensity $\Delta I_{\text{SiNP}}(q, c_{\text{SiNP}})$ for Ludox CL is plotted against q in Figure 7. If we assume Ludox CL in the acetate buffer can be modeled by the polydisperse sphere with log-normal distribution, the form factor is written as

$$P(q) = \frac{\int_0^\infty \Phi^2(qR)w(R)R^3 dR}{\int_0^\infty w(R)R^3 dR} \quad (1)$$

$$\Phi(x) = \frac{3(\sin x - x \cos x)}{x^3} \quad (2)$$

$$w(R) = \frac{1}{\sqrt{2\pi}\sigma_R R} \exp\left\{-\frac{[\ln(R/R_m)]^2}{2\sigma_R^2}\right\} \quad (3)$$

where R_m and σ_R are the parameters of the radius dispersion. If we choose $R_m = 8.9 \text{ nm}$ and $\sigma_R = 0.15$, the calculated $P(q)$ multiplied by a certain constant well reproduce the experimental

data for Ludox CL in the range of $q > 0.3 \text{ nm}^{-1}$. The much smaller R_m value comparing with $R_{H,app}$ indicates that scattering profile in the q range of SAXS mainly reflects the dispersed SiNPs. The upward deviation of the experimental data is most likely because of the aggregation of Ludox CL as in the case of the above-mentioned aggregation behavior observed by SLS and DLS. It should be noted that substantially the same q -dependence was observed at pH 7 (not shown here). Triangles show the excess scattering intensity $\Delta I_x(q, c_x)$ of xanthan solution with the concentration c_x . These concentrations correspond to $c_x/c_{SiNP} = 8.4$. The scattering intensity for the xanthan at the two temperatures can be explained by the wormlike chain model as described in our previous report.^[16]

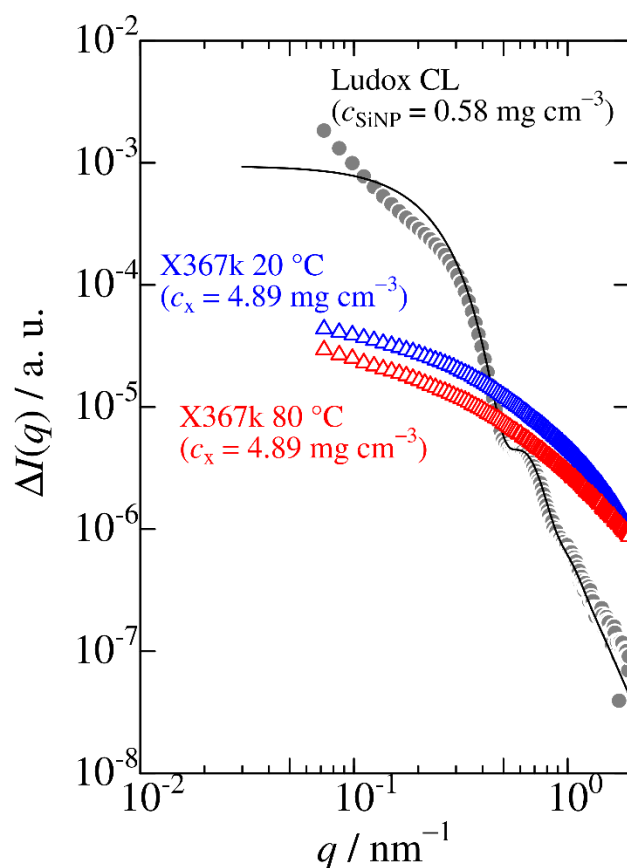


Figure 7. Scattering profile for Ludox CL (circles) compared with those for xanthan at 20 °C (blue triangles) and 80 °C (red triangles).

The scattering intensity $\Delta I_{mix}(\mathbf{q}, \mathbf{c}_{SiNP}, \mathbf{c}_x)$ of the mixed solutions were appreciably stronger than the SiNPs in the low- q region. To discuss this, we introduce the following excess scattering factor $S_E(q)$,

$$S_E(q) = \frac{\Delta I_{mix}(q, c_{SiNP}, c_x)}{\Delta I_{SiNP}(q, c_{SiNP}) + \Delta I_x(q, c_x)} \quad (4)$$

If SiNPs were dispersed in the buffer, $S_E(q)$ could reduce the structure factor. Here, we estimated the scattering intensity of each component $\Delta I_{SiNP}(\mathbf{q}, \mathbf{c}_{SiNP})$ and $\Delta I_x(\mathbf{q}, \mathbf{c}_x)$ from the data in Figure 7 assuming that they are proportional to the concentration in the q range investigated; this may be reasonable because we have checked concentration dependence of the scattering intensity of Ludox CL was negligibly small^[20]. The evaluated $S_E(q)$ data for different conditions are shown in Figure 8. In any cases, $S_E(q)$ is independent of the concentration of xanthan, increases with lowering q in the low q range, and simply approaches unity where $q > 0.3 \text{ nm}^{-1}$. The high scattering intensity in the lowest q region reflects the polyion complex formation of xanthan and Ludox CL. Almost no c_x/c_{SiNP} dependence of $S_E(q)$ may be attributed to that the size of the aggregates does not affect the scattering profile in the q region from our SAXS measurements. However, no region with $S_E(q) < 0.8$ was observed while such region was found for negatively charged SiNP with single chain collagen.^[20] Taking into consideration that such region is related to the densely packed SiNPs, which was estimated from the theoretical analysis in terms of the sticky hard sphere model,^[28] the current $S_E(q)$ result suggests the Ludox CL particles are loosely packed in the aggregate in the both case that xanthan conformation is single chain or double helix.

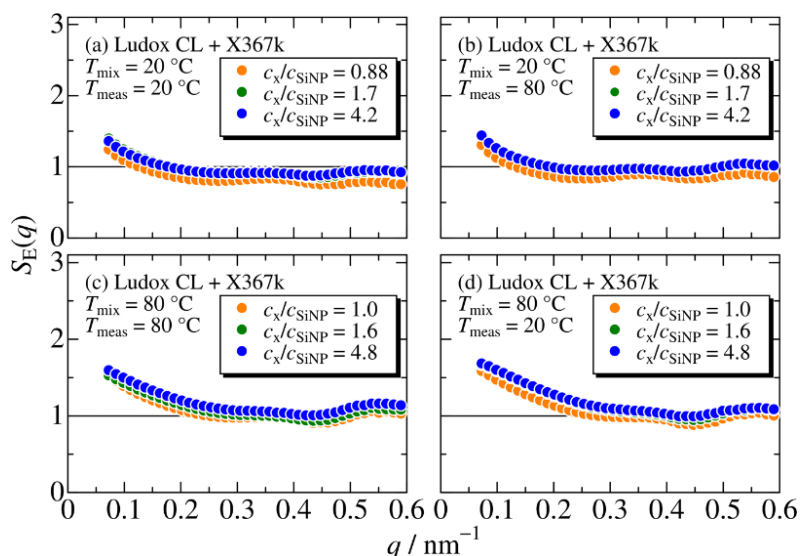


Figure 8. Excess scattering factor $S_E(q)$ for indicated c_x/c_{SiNP} at different mixed and measurement temperatures, T_{mix} and T_{meas} , respectively.

7. Conclusion

In this paper, we investigated polyion complex formation of negatively charged double helical polysaccharide, xanthan, and a positively charged silica nanoparticle, Ludox CL in the acetate buffer at pH 5.0. While xanthan conformation detected by the CD measurement is independent of the concentration of Ludox CL, light scattering intensity became significantly increased with approaching the composition c_x/c_{SiNP} where the ζ potential is inverted. The scattering profile observed by the small angle X-ray scattering supports these results while the silica nanoparticles do not form densely packed structure.

Acknowledgements

The authors are grateful to Prof. Takahiro Sato (Osaka Univ.) for fruitful discussion, and Dr. Noboru Ohta (SPring-8) for SAXS measurements. This work was partly supported by JSPS KAKENHI grant numbers JP20H02788. The synchrotron radiation experiments were performed at the BL40B2 in SPring-8 with the approval of the Japan Synchrotron Radiation Research Institute (JASRI) (proposal nos. 2020A1132, 2020A0529, and 2021A1092).

References

- [1] B. T. Stokke, A. Elgsaeter, O. Smidsrod, *Int. J. Biol. Macromol.* **1986**, *8*, 217.
- [2] B. T. Stokke, O. Smidsrød, A. Elgsaeter, *Biopolymers* **1989**, *28*, 617.
- [3] I. Capron, S. Alexandre, G. Muller, *Polymer* **1998**, *39*, 5725.
- [4] T. A. Camesano, K. J. Wilkinson, *Biomacromolecules* **2001**, *2*, 1184.
- [5] J. Moffat, V. J. Morris, S. Al-Assaf, A. P. Gunning, *Carbohydr. Polym.* **2016**, *148*, 380.
- [6] K. Okuyama, S. Arnott, R. Moorhouse, M. D. Walkinshaw, E. D. T. Atkins, C. H. Wolf-Ullish, "Fiber Diffraction Studies of Bacterial Polysaccharides", in *Fiber Diffraction Methods*, American Chemical Society, 1980, p. 411.
- [7] T. Sato, T. Norisuye, H. Fujita, *Polym. J.* **1984**, *16*, 341.
- [8] T. Sato, S. Kojima, T. Norisuye, H. Fujita, *Polym. J.* **1984**, *16*, 423.
- [9] Y. Matsuda, K. Okumura, S. Tasaka, *Polym. J.* **2018**, *50*, 1043.
- [10] H. Yamakawa, T. Yoshizaki, "*Helical Wormlike Chains in Polymer Solutions, 2nd ed.*", Springer, Berlin, Germany, 2016.
- [11] T. Sato, T. Norisuye, H. Fujita, *Macromolecules* **1984**, *17*, 2696.
- [12] W. Liu, T. Sato, T. Norisuye, H. Fujita, *Carbohydr. Res.* **1987**, *160*, 267.
- [13] W. Liu, T. Norisuye, *Int. J. Biol. Macromol.* **1988**, *10*, 44.
- [14] W. Liu, T. Norisuye, *Biopolymers* **1988**, *27*, 1641.
- [15] S. Kitamura, K. Takeo, T. Kuge, B. T. Stokke, *Biopolymers* **1991**, *31*, 1243.
- [16] Y. Tomofuji, K. Matsuo, K. Terao, *Carbohydr Polym* **2022**, *275*, 118681.
- [17] M.-H. Oh, J.-H. So, S.-M. Yang, *J. Colloid Interface Sci.* **1999**, *216*, 320.
- [18] G. Pi, Y. M. Li, M. T. Bao, L. L. Mao, H. Y. Gong, Z. N. Wang, *ACS Sustain. Chem. Eng.* **2016**, *4*, 3095.
- [19] A. Verma, G. Chauhan, P. P. Baruah, K. Ojha, *Ind. Eng. Chem. Res.* **2018**, *57*, 13449.
- [20] K. Terao, M. Otsubo, M. Abe, *Langmuir* **2020**, *36*, 14425.
- [21] P. Van der Meeren, H. Saveyn, S. Bogale Kassa, W. Doyen, R. Leysen, *Phys. Chem. Chem. Phys.* **2004**, *6*, 1408.
- [22] M. Otsubo, K. Terao, *Polym. J.* **2021**, *53*, 1481.
- [23] N. Shimizu, K. Yatabe, Y. Nagatani, S. Saijyo, T. Kosuge, N. Igarashi, *AIP Conference Proceedings* **2016**, *1741*, 050017.
- [24] M. Kanao, Y. Matsuda, T. Sato, *Macromolecules* **2003**, *36*, 2093.
- [25] K. Ueno, H. Ueno, T. Sato, *Polym. J.* **2012**, *44*, 59.
- [26] H. D. Liu, T. Sato, *Chin. J. Polym. Sci.* **2013**, *31*, 39.
- [27] M. M. Tirado, C. L. Martínez, J. G. de la Torre, *J. Chem. Phys.* **1984**, *81*, 2047.
- [28] R. J. Baxter, *J. Chem. Phys.* **1968**, *49*, 2770.